ORIGINAL PAPER

Igor Schepetkin · Andrei Potapov · Andrei Khlebnikov
Elena Korotkova · Anna Lukina · Galina Malovichko
Lilia Kirpotina · Mark T. Quinn

Decomposition of reactive oxygen species by copper(II) bis(1-pyrazolyl)methane complexes

Abstract Two bis(1-pyrazolyl)alkane ligands, bis(3,5-dimethyl-1-pyrazolyl)methane and bis(4-iodo-3,5-dimethyl-1-pyrazolyl)methane, and their copper(II) complexes, bis(3,5-dimethyl-1-pyrazolyl)methanedinitratocopper(II) $[CuL_1(NO_3)_2]$ and bis(4-iodo-3,5-dimethyl-1-pyrazolyl)methanedinitratocopper(II) $[CuL_2(NO_3)_2] \cdot 2H_2O$, were prepared. Physiochemical properties of the copper(II) complexes were studied by spectroscopic (UV–vis, IR, EPR) techniques and cyclic voltammetry. Spectroscopic analysis revealed a 1:1 stoichiometry of ligand:copper(II) ion and a bindentate coordination mode for the nitrate ions in both of the complexes. According to experimental and theoretical ab initio data, the copper(II) ion is located in an octahedral hexacoordinated environment. Both complexes were able to catalyze the dismutation of superoxide anion $(O_2^{\bullet-})$ (pH 7.5) and decomposition of H_2O_2 (pH 7.5) and peroxynitrite (pH 10.9). In addition, both complexes exhibited superoxide dismutase (SOD) like activity toward extracellular and intracellular reactive oxygen species produced by activated human neutrophils in whole blood. Thus, these complexes represent useful SOD mimetics with a broad range of antioxidant activity toward a variety of reactive oxidants.

I. Schepetkin · L. Kirpotina · M. T. Quinn (✉)
Department of Veterinary Molecular Biology,
Montana State University, Bozeman,
MT 59717, USA
E-mail: mquinn@montana.edu
Tel.: +1-406-9945721
Fax: +1-406-9944303

A. Potapov · A. Khlebnikov
Department of Chemistry, Altai State Technical University,
Barnaul, Russia

E. Korotkova · A. Lukina
Department of Chemical Technology,
Tomsk Polytechnic University,
Tomsk, Russia

G. Malovichko
Department of Physics,
Montana State University, Bozeman,
MT 59717, USA

Introduction

Reactive oxygen species (ROS) are produced during normal cellular metabolism and are essential in many biochemical processes, including intermolecular and intracellular signaling, cell growth and differentiation, and host defense mechanisms (reviewed in [1, 2]). Conversely, excessive ROS production leads to oxidative stress and host tissue damage, and cells have developed both enzymatic and nonenzymatic antioxidant defense mechanisms to protect against the detrimental effects of ROS [3, 4]. Among the most prominent enzymatic antioxidant mechanisms are superoxide dismutases (SOD), which catalyze the dismutation of superoxide anion $(O_2^{\bullet-})$ to O_2 and hydrogen peroxide (H_2O_2); catalases, which convert H_2O_2 to H_2O; and peroxidases, which also eliminate H_2O_2 [4–6]. Because of the importance of antioxidant defenses in health and disease, a significant amount of research has focused on the understanding of these defense mechanisms, as well as on the development of potential therapeutic antioxidant compounds.

One successful approach to understanding SOD function has been the development of model compounds that mimic SOD properties [7], and low molecular weight metal chelates have been shown to mimic SOD catalytic activity [8–10]. It is clear that the active site of SOD, as well as a number of other copper-containing proteins, such as laccase, galactose oxidase, and ascorbate oxidases, could be partly mimicked by simple models containing pyrazole rings. For example, copper complexes coordinated to polydentate pyrazole-based ligands have been proposed as models for the type-3 active site of the copper proteins hemocyanin and tyrosinase [11].

The coordination properties of pyrazole ligands can be altered widely by introducing various substituents

into the pyrazole rings, and this property has been exploited in the search for useful enzyme mimics. For example, both poly(1-pyrazolyl)alkanes and their transition metal complexes are known to demonstrate biological activity [12–14]. Bis(1-pyrazolyl)alkanes generally act as bidentate chelating ligands, and bis(1-pyrazolyl)methanes represent a class of versatile N_2-donor chelating ligands that form complexes with both transition and main-group elements [15]. Indeed, complexes of bis(1-pyrazolyl)methanes bearing substituents at the CH_2 bridge with Zn^{2+} [16, 17], Fe^{2+} [17], Co^{2+} [18], Ni^{2+} [19], and Cu^{2+} [20] have been reported to serve as biomimetic models of metalloenzymes.

The effects of bis(3,5-dimethyl-1-pyrazolyl)methane (L_1) copper(II) complexes on ROS decomposition have not been studied so far, although two such compounds have been reported in the literature. Reedijk and Verbiest [21] prepared a 1:2 complex $[Cu(L_1)_2(NO_3)_2]$ and proposed an octahedral coordination center with two bindentate chelating L_1 ligands and two monodentate nitrate ions coordinated in *cis* positions. Similarly, Mesubi and Anumba [22] reported the isolation of a 1:1 complex from a methanol solution. IR spectra for this complex were indicative of monocoordinated nitrate ions, giving rise to a CuO_2N_2 chromophore.

In the present report, we describe the synthesis of L_1 and its previously unknown 4,4′-diiodo derivative. Furthermore, spectroscopic, electrochemical, and biochemical properties of copper(II) complexes of these ligands are presented, including evaluation of SOD-like activity, effects on H_2O_2 and peroxynitrite decomposition, and effects on ROS production by human neutrophils.

Experimental

Materials

Commercial reagents and solvents were used as obtained without further purification. 8-Amino-5-chloro-7-phenylpyridol[3,4-*d*]pyridazine-1,4(2*H*,3*H*)-dione (L-012) was purchased from Wako Chemicals (Richmond, VA, USA). Sodium peroxynitrite was purchased from Calbiochem (La Jolla, CA, USA). SOD from horseradish, phorbol-12-myristate-13-acetate (PMA), zymosan A from *Saccharomyces cerevisiae*, luminol, xanthine oxidase, xanthine, phenazine methosulfate (PMS), NADH, nitro blue tetrazolium (NBT), and dihydrorhodamine (DHR) 123 were purchased from Sigma Chemical Co. (St. Louis, MO, USA).

Synthesis of bis(3,5-dimethyl-1-pyrazolyl)methane

L_1 was prepared as previously described [23]. Briefly, 5.00 g (52.1 mmol) 3,5-dimethylpyrazole was dissolved in 50 ml dimethyl sulfoxide (DMSO), and 5.84 g (104.2 mmol) of finely powdered KOH was added. The suspension was vigorously stirred for 1 h at 80 °C, and 4.53 g (1.8 ml, 26.1 mmol) dibromomethane in 10 ml DMSO was added dropwise over 30 min. Stirring at 80 °C was continued for an additional 4 h, and the reaction mixture was poured into 200 ml H_2O and extracted with chloroform (4 × 40 ml). The extract was washed with H_2O (2 × 20 ml) and dried over anhydrous calcium chloride. Removal of the solvent produced 4.90 g (yield 92%) of solid product, which was purified by crystallization from benzene/hexane (1:1), melting point 105–105.5 °C. Elemental analysis calculated for $C_{11}H_{16}N_4$ (%): C, 64.68; H, 7.89; N, 27.43. Found: C, 63.88; H, 8.03; N, 26.82. ^{1}H NMR (DMSO-d_6, 300 MHz, δ, ppm): 2.05 (6H, 3-CH_3-pz), 2.39 (6H, 5-CH_3-pz), 6.29 (2H, H_4-pz), 6.40 (2H, CH_2).

Synthesis of bis(4-iodo-3,5-dimethyl-1-pyrazolyl)methane

A suspension of 4.08 g (20.0 mmol) of L_1, 4.06 g (16.0 mmol) of powdered iodine, and 1.41 g (8.0 mmol) HIO_3 in 50 ml glacial acetic acid and 5 ml of 30% aqueous H_2SO_4 was vigorously stirred for 30 min at room temperature until the reaction mixture became colorless. The mixture was then poured into 250 ml H_2O, and the precipitate was filtered, washed with H_2O, and dried to yield 8.55 g (94%) bis(4-iodo-3,5-dimethyl-1-pyrazolyl)methane (L_2) (colorless crystals), melting point 183–184 °C (EtOH). Elemental analysis calculated for $C_{11}H_{14}N_4I_2$ (%): C, 29.27; H, 3.09; N, 12.28. Found: C, 29.34; H, 3.04; N, 12.08. ^{1}H NMR (CDCl$_3$, 300 MHz, δ, ppm): 2.12 (6H, 3-CH_3-pz), 2.40 (6H, 5-CH_3-pz), 6.08 (2H, CH_2).

Synthesis of bis(3,5-dimethyl-1-pyrazolyl)methanedinitratocopper(II)

Bis(3,5-dimethyl-1-pyrazolyl)methanedinitratocopper(II) (complex **1**) was obtained by mixing Cu(NO$_3$)$_2$·6H$_2$O (0.888 g, 3.0 mmol) in acetone (3 ml) with L_1 (0.612 g, 3.0 mmol) in the same solvent (3 ml). The blue precipitate immediately formed was filtered after 30 min and washed several times with acetone to yield 1.09 g (93%) of complex **1**, melting point 230–231 °C, decomposed. Elemental analysis calculated for $(C_{11}H_{16}N_4)Cu(NO_3)_2$ (%): C, 33.72; H, 4.12; N, 21.45; Cu, 16.22. Found: C, 34.20; H, 4.45; N, 20.98; Cu, 16.00.

Synthesis of bis(4-iodo-3,5-dimethyl-1-pyrazolyl)methanedinitratocopper(II)

Bis(4-iodo-3,5-dimethyl-1-pyrazolyl)methanedinitratocopper(II) (complex **2**) was prepared similarly from 0.65 g (2.19 mmol) Cu(NO$_3$)$_2$·6H$_2$O in 6 ml acetone and 1.00 g (2.19 mmol) of L_2 in 30 ml of the same solvent. Green crystals of complex **2** (1.32 g, yield 94%; melting point 222–223 °C, decomposed) were obtained. Elemental

analysis calculated for $(C_{11}H_{14}N_4I_2)Cu(NO_3)_2 \cdot 2H_2O$ (%): C, 19.44; H, 2.67; N, 12.37; I, 37.34; Cu, 9.35. Found: C, 19.82; H, 2.95; N, 12.09; I, 36.75; Cu, 9.37.

Spectroscopy

IR spectra were recorded from 4,600 to 650 cm^{-1} with a Specord 71 IR spectrophotometer (Carl Zeiss, Germany) using KBr pellets. NMR spectra were recorded using a Bruker AV300 spectrometer (Bruker BioSpin, Ettlingen, Germany). UV–vis spectra were collected with a SpectraMax Plus spectrophotometer (Molecular Devices, Sunnyvale, CA, USA). The EPR spectra of solid-state samples at room temperature were obtained with a Bruker ELEXSYS 560 EPR/electron–nuclear double resonance spectrometer operating at the Q-band frequency of 34 GHz. Parameters of the **g** tensor and the hyperfine tensor (**A**) of the complexes were obtained by simulation of the spectra. A computer simulation of the powder-EPR spectra was written by V. Grachev (Department of Physics, Montana State University, Bozeman, MT, USA) and is based on exact numerical diagonalization of the spin-Hamiltonian matrix. The best-fit procedure was verified by simulation of EPR spectra of the copper complexes reported by Patel et al. [24].

Cyclic voltammetry

Cyclic voltammetric measurements were performed at 25 °C under a nitrogen atmosphere using a TA-2 voltammetric analyzer (Tomanalyte, Russia) at a scan rate of 50 mV s^{-1} in aqueous ethanol solution (10%). A 3-mm-diameter glassy-carbon working electrode, an Ag/AgCl reference electrode, and a Pt-wire counter electrode were used in a glass cell (0.025 M of phosphate buffer solution as a supporting electrolyte). Electrochemical potentials were converted to the normal hydrogen electrode (NHE). The half-wave potentials $E_{1/2}$ were calculated approximately from $(E_{pa} + E_{pc})/2$.

Molecular modeling

Semiempirical calculations were performed using the PM3 method, as implemented in HyperChem [25]. The molecular structures were generated with the molecular builder supplied in the HyperChem package and optimized in vacuo using the Polak–Ribiere (conjugate gradient) algorithm until a root-mean-square gradient less than 10 cal Å^{-1} mol^{-1} was attained. The geometric parameters obtained were used as starting values for ab initio geometry optimizations in a 3-21G basis set. All calculations were carried out at unrestricted Hartree–Fock level for the doublet lowest-energy state with no configuration interaction and electron correlation imposed, and a convergence limit for the self-consistent-field (SCF) procedures at 10^{-5} au.

SOD-like activity

Superoxide anion ($O_2^{\bullet-}$) was generated in enzymatic (xanthine/xanthine oxidase) and nonenzymatic (PMS/NADH) systems in the presence or absence of test compounds, and $O_2^{\bullet-}$ production was determined by monitoring reduction of NBT to monoformazan dye at 560 nm. The enzymatic system consisted of 500 μM xanthine, 500 μM NBT, 3.75 mU ml^{-1} xanthine oxidase, and 0.1 M phosphate buffer (pH 7.5), whereas the nonenzymatic system contained 3 μM PMS, 200 μM NADH, and 50 μM NBT in 0.05 M phosphate buffer (pH 7.5) [26]. The reactions were monitored at 560 nm with a SpectraMax Plus microplate spectrophotometer at 25 °C, and the rate of absorption change was determined. The concentration required to produce 50% inhibition (IC$_{50}$) was obtained by graphing the rate of NBT reduction versus the logarithm of the concentration of the copper compound. A kinetics constant k_{cat} was calculated using the equation $k_{cat} = k_{NBT}[NBT]/IC_{50}$, where $k_{NBT} = 5.94 \times 10^4 M^{-1} s^{-1}$ is a second-order rate constant for a NBT [27, 28]. To evaluate if the experimental compounds affected the generation of $O_2^{\bullet-}$ by direct interaction with xanthine oxidase, enzyme activity was evaluated by spectrophotometric measurement of uric acid formation from xanthine at 295 nm [29]. The reaction mixtures contained 500 μM xanthine, 3.75 mU ml^{-1} xanthine oxidase, and 0.1 M phosphate buffer (pH 7.5), and the reactions were monitored in the presence or absence of test compounds.

SOD-like activity of the copper compounds was also evaluated by measuring the concentration-dependent decrease in electrochemical reduction current of oxygen at a mercury film electrode (MFE) after reaction of the compounds with $O_2^{\bullet-}$ [30]. Voltammograms of the cathodic reduction of O_2 were recorded with the TA-2 voltammetric analyzer using differential pulse voltammetry under the following conditions: potential scan rate 50 mV s^{-1}, potential range $E = 0$ to -1.0 V, and amplitude 10 mV. The electrochemical cell consisted of a working MFE, a silver/silver chloride reference electrode with saturated KCl (Ag|AgCl|KCl$_{sat}$), and a nitrogen supply tube. It should be noted that the reduction peak of the copper(II) compounds tested was observed at $E = -0.1$ V versus Ag,AgCl/Cl$^-$ and did not overlap with the electrochemical reduction peak of O_2 at $E = -0.35$ V.

Peroxidase-like activity

Peroxidase-like activity of the copper compounds was determined by evaluating their ability to reduce H_2O_2, forming hydroxyl radical (OH$^{\bullet}$), which was detected with luminol or a highly sensitive chemiluminescent

probe, L-012 [31, 32]. Stock H_2O_2 was stored in the dark at 4 °C, and the concentration was determined before measurements using a molar extinction coefficient of 81 M^{-1} cm^{-1} at 230 nm. Reaction mixtures containing H_2O_2, test compounds, and 50 μM L-012 or 25 μM luminol were added to black 96-well microtiter plates, and luminescence was monitored using a Fluoroscan Ascent FL microplate reader (Thermo Electron Corp., Milford, MA, USA) at 25 °C.

Peroxynitrite decomposition

Sodium peroxynitrite was stored in small aliquots at −80 °C. The peroxynitrite stock was diluted with 0.1 M NaOH, and the concentration of the resulting solutions was determined spectrophotometrically prior to each experiment by measuring the absorbance at 302 nm ($\varepsilon_{302} = 1{,}705$ M^{-1} cm^{-1} [33]). Kinetics reactions were carried out at 25 °C in 0.1 M phosphate buffer at a final pH of 10.9, and peroxynitrite decay was monitored at 302 nm, using a SpectraMax Plus spectrophotometer. Michaelis–Menten data were obtained by linear fits over the first 25% of the reaction and were corrected for background decay by similar fits to data recorded in the absence of catalyst. Peroxynitrite-mediated oxidation of DHR 123 to rhodamine 123 [34] was measured using a Fluoroscan Ascent FL microplate reader at 485-nm excitation and 538-nm emission. Briefly, 80 μM peroxynitrite was added to 15 μM DHR 123 in the presence or absence of test copper compounds, and fluorescence was measured immediately. All fluorescence intensities measured were corrected for background fluorescence (sample fluorescence without peroxynitrite).

Neutrophil ROS production

Human blood was collected from healthy volunteers into heparin-containing Vacutainer tubes (BD Biosciences, Franklin Lakes, NJ, USA) in accordance with a protocol approved by the Institutional Review Board at Montana State University. The blood was diluted 1:1,000 in Hanks's balanced-salt solution (pH 7.4) without phenol red, and spontaneous chemiluminescence was monitored at 37 °C for 1 h in the presence of 50 μM L-012. Chemiluminescence was also monitored after treatment of the cells with serum-opsonized zymosan particles (100 μg ml^{-1}) or 200 nM PMA, each ±1 U ml^{-1} SOD.

Cell proliferation and cytotoxicity assay

The mouse macrophage cell line J774.A1 was grown in Dulbecco's modified Eagle's medium (DMEM) supplemented with 10% (v/v) bovine serum, 100 μg ml^{-1} streptomycin, and 100 U ml^{-1} penicillin, and was incubated at 37°C in a humidified atmosphere containing 5% CO_2. Cells were grown to confluence in sterile tissue culture flasks and gently detached by scraping. Cell number and viability were assessed microscopically using trypan blue exclusion.

Cell proliferation and cytotoxicity were analyzed by measuring ATP [35] with the CellTiter-Glo Luminescent Cell Viability Assay kit (Promega, Madison, WI, USA), according to the manufacturer's protocol. J774.A1 cells (25,000 cells per well) were suspended in phenol red free DMEM supplemented with 3% (v/v) bovine serum, 100 μg ml^{-1} streptomycin, and 100 U ml^{-1} penicillin, seeded in 96-well microtiter plates (Costar, Milpitas, CA, USA), and were treated with test compounds for 18 h. Half an hour before the end of the treatment, the cells were allowed to equilibrate to room temperature, substrate was added, and the samples were analyzed with a Fluoroscan Ascent FL microplate reader.

Results and discussion

Synthesis

Development of the coordination chemistry of poly(pyrazolyl)alkanes has been limited by the complexity of the synthetic procedures required to prepare these ligands. Previously, Trofimenko [10] reported procedures for the preparation of bis(1-pyrazolyl)methane by heating pyrazole with dibromomethane in an autoclave at 150 °C or by the reaction of pyrazole with methyl orthoformate; however, the yields were not optimal (46 and 75% yield, respectively). More recently, Julia and coworkers [36, 37] prepared a series of substituted poly(1-pyrazolyl)methane derivatives in higher yields (78–93%) using a reaction between pyrazoles and dihalogenoderivatives of hydrocarbons under phase-transfer conditions, suggesting this could be a versatile method for the preparation of geminal polyazolylalkanes; however, reaction times were excessive, requiring 24 h for completion.

We report here the development of a novel, highly efficient procedure for the double alkylation of azoles, which involves their reaction with halogeno derivatives in a superbasic medium (KOH/DMSO system). Using this method, bis(3,5-dimethyl-1-pyrazolyl)methane (L_1) was prepared as shown in Scheme 1. The reaction of 3,5-dimethylpyrazole with dibromomethane provided the desired product with an excellent yield (92%), and the duration of the synthesis was only 4 h at 80 °C.
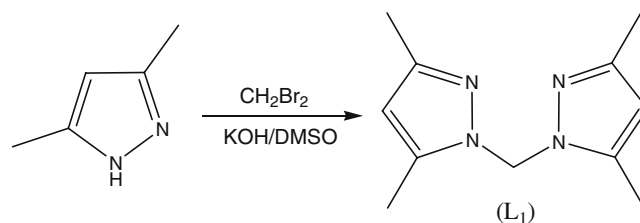
Scheme 1 Preparation of bis(3,5-dimethyl-1-pyrazolyl)methane (L_1)

Furthermore, dibromomethane can be substituted by the less expensive and less toxic dichloromethane without a decrease in yield. Importantly, this method does not require the use of environmentally harmful solvents and catalysts. Thus, this method represents a simpler and more effective approach for preparing bis(1-pyrazolyl)methane and derivatives.

Bis(4-iodo-3,5-dimethyl-1-pyrazolyl)methane (L_2) was prepared by oxidative iodination of L_1 using an I_2/HIO$_3$/H$_2$SO$_4$ mixture in acetic acid. Previously, this system appeared to give good results for iodination of various substituted *N*-methylpyrazoles [38]. Likewise, the iodination of L_1 proceeded at room temperature, readily generating L_2 at 94% yield (Scheme 2).

Cu(II) complexes of L_1 and L_2 were obtained in high yields (93–94%) by their reaction with Cu(NO$_3$)$_2$·6H$_2$O in acetone solution. Elemental analysis of the complexes demonstrated 1:1 stoichiometry, indicating the molecular formulas for complexes **1** and **2** were CuL$_1$(NO$_3$)$_2$ and CuL$_2$(NO$_3$)$_2$·2H$_2$O, respectively. Further spectroscopic analysis of L_1 and L_2 and their copper complexes is described in the following.

IR spectra

The characteristic bands in the IR spectra of the free ligands and their complexes are shown in Table 1. The IR spectra of complex **2** exhibited a broad band in the 3,400–3,200 cm^{-1} region and a band at 1,690 cm^{-1}, which are due to stretching and bending vibrations of an O–H bond and are indicative of the presence of H$_2$O molecules in this complex. The bands in the 1,560–1,330 cm^{-1} area corresponding to pyrazole breathing vibrations generally showed a slight shift toward lower frequencies upon coordination to Cu^{2+} ion. In addition, considerable changes in absorption intensity due to bending vibrations of C−H bonds were observed in the "fingerprint" area. In the spectra of complexes **1** and **2**, three strong bands due to vibrations of the nitrate ion possessing a C_{2v} symmetry were detected, and the large separation between two high-frequency bands (1,500–1,280 and 1,470–1,300 cm^{-1}, respectively) suggested a bidentate coordination mode for the nitrate ions in both of the complexes [39]. The bands at 730 and 725 cm^{-1} were assigned to the bending vibrations (δ_{N-O}) of the NO$_3^-$ ion [39].

Electronic absorption

The absorbance bands detected by UV–vis spectroscopy of the ligands and their copper complexes in ethanol are presented in Table 1. The UV spectra of the ligands each contained two absorption maxima, with peaks at 206 and 222 nm and at 204 and 238 nm for L_1 and L_2, respectively. In comparison, the UV spectrum of complex **1** exhibited a single absorption maximum at 208 nm, while the spectrum for complex **2** had maxima at 204 and 234 nm. These peaks are presumably due to intraligand excitation, while the peaks at 282 and 343 nm for complex **1** and at 342 nm for complex **2** appear have ligand-to-metal charge-transfer origin [40, 41].

The visible spectra of complexes **1** and **2** were characterized by a broad absorbance, with shoulder bands at 932 and 1,030 nm and peaks centered at 708 and 722, respectively. This absorbance can be attributed to $d \rightarrow d^*$ transitions involving Cu(II) ions bound to a distorted octahedral hexacoordinated N$_2$O$_4$ chromophore [40]. Furthermore, comparison of electronic spectral parameters of the Cu(II) center in complexes **1** and **2** with those of Cu$_2$Zn$_2$SOD ($\lambda_{max} = 685$ nm, $\varepsilon = 150$ M^{-1} cm^{-1} [42]) indicated complex **1** was more similar than complex **2** to the Cu(II) center of Cu$_2$Zn$_2$SOD. The visible spectrum of Cu(NO$_3$)$_2$ contained a single peak at 792 nm (data not shown).

As indicated by spectroscopic measurements, we obtained an octahedral copper complex from acetone solution. In contrast, Mesubi and Anumba [22] reported the preparation of a tetrahedral complex from methanol solution. The difference in the structures of these complexes was confirmed by their distinct melting points (225–227 °C for the tetrahedral complex vs. 230–231 °C for complex **1**) and spectroscopic characteristics. For example, spectra of the tetrahedral complex showed a d–d^* absorption at 740 nm [22], while the octahedral complex **1** absorbed at 708 nm. It should be noted that an octahedral Cu(L$_1$)$_2$(NO$_3$)$_2$ complex reported by Reedijk and Verbiest [21] exhibited two absorption maxima at 1,042 and 694 nm.

Electron paramagnetic resonance

Q-band EPR spectra of solid-state samples were recorded at room temperature. In Fig. 1 the EPR spectra

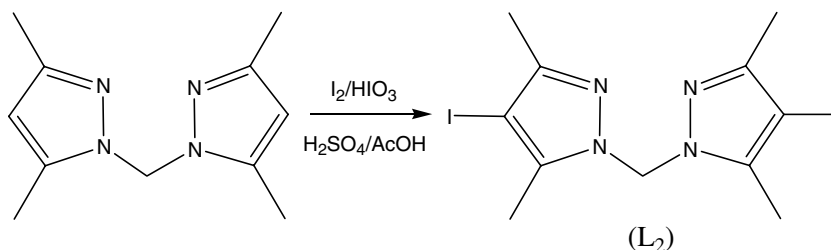**Scheme 2** Preparation of bis(4-iodo-3,5-dimethyl-1-pyrazolyl)methane (L_2)

Table 1 Selected IR and UV–vis data of the free ligands and their Cu(II) complexes

Compound	IR data (cm^{-1})					UV–vis data
	ν_{O-H}, δ_{O-H}	ν_{C-H}	Pyrazole ring vibrations	δ_{C-H}	Nitrate ion	λ, nm (ε, M^{-1} cm^{-1})
L$_1$	–	2,900b	1,550s, 1,450s, 1,345s	795s, 765s, 700 m, 660s	–	206 (5,904) 222 (6,788)
Complex **1**	–	2,930b	1,540s, 1,455s,	820m, 795s, 760s, 690w, 665s	1,500s, 1,280s, 1,040m, 730w	208 (80,300) 282 (4,896) 343^a 708 (148) 932^a
L$_2$	–	2,890b	1,525s, 1,460s, 1,370m, 1,335s	820s, 710m, 670s	–	204 (6,559) 238 (6,789)
Complex **2**	3,370b, 1690m	2,890b	1,520m, 1,370s	835m, 790w, 700w, 675m	1,470s, 1,300s, 1,000s, 725w	204 (27,650) 234 (13,860) 342^a 722 (50) 1,030^a

^{a}Shoulder region

of complexes **1** and **2** with the simulations that eventually gave the best fit are shown. Zeeman splitting and hyperfine interaction for two isotopes of Cu^{2+} were taken into account in the simulation. The original line of every hyperfine component of the EPR spectrum had a Lorentzian shape with the line width Δ, which did not depend on the orientation of the external magnetic field.
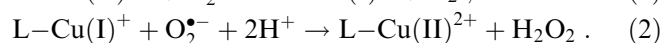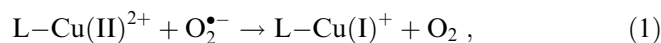
Complex **1** had a nearly axial symmetry, with tensor values $g_\perp = 2.0875$, $g_{||} = 2.325$, $A_\perp < 50 \times 10^{-4}$ cm^{-1}, and $A_{||} = 140 \times 10^{-4}$ cm^{-1}. These parameters are typical values for hexacoordinated copper complexes in an axial elongated octahedral environment, since $g_{||} > g_\perp$; $|A_\perp| < |A_{||}| \approx (120{-}200) \times 10^{-4}$ cm^{-1} [43–45]. The difference between the simulated and experimental spectra at low magnetic fields could probably be explained by the presence of additional superhyperfine interactions of copper electrons with nitrogen atoms N(3) and N(10) of L$_1$. The features of the EPR spectrum of complex **2** with tensor values $g_{xx} = 2.0875$, $g_{yy} = 2.144$, $g_{zz} = 2.26$, $A_{xx} \leq 10$, $A_{yy} \leq 40$, and $A_{zz} \leq 50$ (in 10^{-4} cm^{-1}) were very different from those of complex **1**. These data indicate the Cu^{2+} in complex **2** had a low-symmetry surrounding. Low-symmetry distortions may be due to H$_2$O molecules in complex **2**, which cause alternations in its structure when they are packed together in a crystal lattice. This may also lead to the appearance of several different species of copper complexes with diverse geometry, which have unequal values of g factors in crystals. Significant reduction of hyperfine interaction (indicated by decreased line widths) usually appears in coupled pairs of Cu^{2+} with a strong exchange interaction [43]. Therefore, we cannot exclude the additional presence of such pairs in complex **2**.

Electrochemical properties

The redox potential of Cu(II) complexes is an important factor contributing to SOD-like activity [45]. Therefore, we evaluated the electrochemical properties of our complexes. Cyclic voltammograms were collected for complexes **1** and **2** in aqueous ethanol under an N$_2$ atmosphere (Fig. 2). The complexes showed quasi-reversible one-electron redox potentials, with a pair of cathodic and anodic waves of the Cu(II)/Cu(I) couple in the range between −20 and 382 mV (vs. NHE) (Table 2). The redox potentials of complexes **1** and **2** were different from each other, and complex **2** exhibited a lower cathodic wave potential compared with complex **1** and Cu(NO$_3$)$_2$ (Table 2), which is generally characteristic of iodine-containing compounds [46].

In order to catalyze O$_2^{\bullet-}$ dismutation, the complex must have a half-wave potential within the following range: -0.16 V $< E^\circ < 0.89$ V [42]. For complex **1**, $E_{1/2} = 0.303$ V (vs. NHE) and for complex **2**, $E_{1/2} = 0.151$ V (vs. NHE). Therefore, both complexes can undergo a reduction by O$_2^{\bullet-}$, and their reduced forms can be re-oxidized by O$_2^{\bullet-}$ to finish the catalytic cycle, although complex **1** should be more active owing to a higher redox potential and a greater reversibility of the electrode process [8], as follows:

$$L-Cu(II)^{2+} + O_2^{\bullet-} \rightarrow L-Cu(I)^+ + O_2 , \qquad (1)$$
$$L-Cu(I)^+ + O_2^{\bullet-} + 2H^+ \rightarrow L-Cu(II)^{2+} + H_2O_2 . \qquad (2)$$

Molecular modeling

The energies of boundary orbitals in molecules are known to correlate with their redox properties, including reactivity with O$_2^{\bullet-}$ [47]. To obtain preliminary information on the structure and reactivity of our complexes, we performed ab initio SCF calculations using octahedrally coordinated Cu(II) centers as starting structures for geometry optimization.

The coordination polyhedrons of Cu(II) were composed of N$_2$-bidentate chelating ligands L$_1$ or L$_2$ and
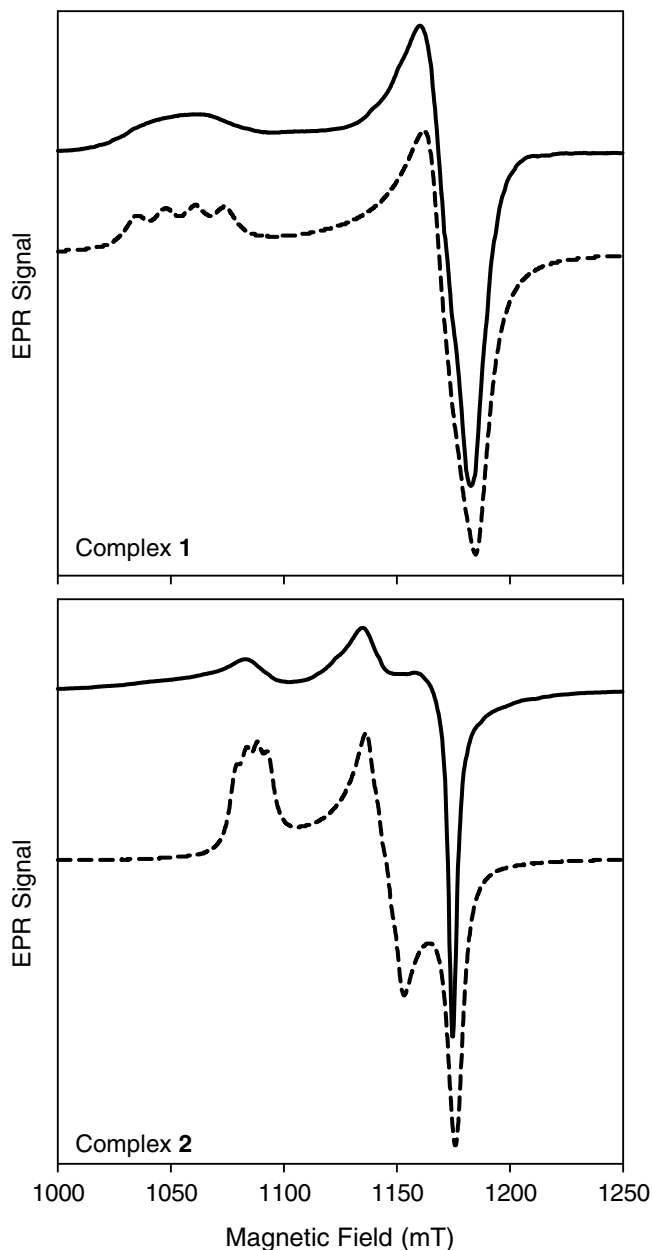
On the basis of our modeling data, it appears that a bidentate chelating coordination of NO_3^- ions is more favorable, with complex **1** being thermodynamically more stable than complex **2**. The connectivity (bond orders) of the bispyrazole ligand-to-copper(II) center is also higher for complex **1**. Therefore, complex **1** should be more stable than the complex of iodo-derivative L_2. Consequently, higher reactivity toward $O_2^{\bullet-}$ should be expected for complex **1** [40]. Furthermore, the LUMO of compound **1** is somewhat lower than that of complex **2**, which is consistent with the more positive reduction potential of complex **1** determined by cyclic voltammetry (Fig. 2). The lower energy level of a LUMO orbital is also indicative of a higher reactivity in $O_2^{\bullet-}$ dismutation reactions [47].

SOD-like activity

Our preliminary data indicated that the copper complexes **1** and **2** [as well as $Cu(NO_3)_2$] exerted a striking SOD-like activity in a xanthine/xanthine oxidase assay. However, the IC_{50} values for inhibition of NBT reduction and uric acid production in this system were quite close (Table 6), indicating the enzymatic assay would not be able to provide conclusive evidence regarding SOD-like activity of our compounds. Furthermore, a small amount of $O_2^{\bullet-}$ is produced in the xanthine/xanthine oxidase system. Thus, we were not able to use this system to distinguish between catalytic and stoichiometric scavenger effects of our compounds, which is consistent with studies of Policar et al. [48], who reported this was a problem for compounds showing IC_{50} values greater than 1 μM in the xanthine/xanthine oxidase assay system. Therefore, we addressed this issue using nonenzymatic assay systems.

SOD-like activity of the Cu(II) complexes was compared with the activity of authentic SOD in a nonenzymatic $O_2^{\bullet-}$-generating system (PMS/NADH system), as well as in an electrochemical reduction assay. In both systems, complex **1** exhibited potent SOD-like activity, which was greater than that of complex **2** and $Cu(NO_3)_2$ (Fig. 4, Table 6). Complex **2** demonstrated moderate SOD-like activity, which was slightly higher than that of $Cu(NO_3)_2$. Although complexes **1** and **2** ($IC_{50} = 4.5 \times 10^{-7}$ and 7.9×10^{-7} M, respectively) were not as effective as horseradish SOD ($IC_{50} = 7 \times 10^{-8}$ M) (Fig. 4) or bovine erythrocyte SOD ($IC_{50} = 4 \times 10^{-8}$ M) [49], their activities were on the same order of magnitude as the best SOD analogues described in the literature [9, 28, 42]. The lower k_{cat} of $Cu(NO_3)_2$ compared with that of the two complexes suggests that the activity of the complexes was not due to their dissociation in solution. It should be noted that both ligands, L_1 and L_2, did not exhibit any $O_2^{\bullet-}$-scavenger effects over the same concentration range (0.1–100 μM) in either the enzymatic or the nonenzymatic $O_2^{\bullet-}$-generating systems (data not shown). Therefore, our data demonstrate both complexes can

Fig. 1 EPR spectra of Cu(II) complexes. Experimental (*solid lines*) and simulated (*dashed lines*) EPR spectra of complexes **1** (*upper panel*) and **2** (*lower panel*) recorded at room temperature. Lorentzian line widths $\Delta(\mathbf{1}) = 8 \times 10^{-4}$ cm^{-1}, $\Delta(\mathbf{2}) = 4 \times 10^{-4}$ cm^{-1}

two O_2-bidentate chelating nitrate ions. A molecular representation of the complexes, together with the atomic labeling schemes, is shown in Fig. 3, and corresponding structural data are presented in Tables 3 and 4. Notably, the values of the bond distances and angles agreed with those reported previously in X-ray diffraction studies of similar copper complexes [11, 44]. Table 5 contains the energies of boundary orbitals (highest occupied molecular orbital; lowest unoccupied molecular orbital, LUMO) of the complexes determined from ab initio calculations, as well as the heats of formation calculated both for monodentate and bidentate coordination modes of nitrate ions.
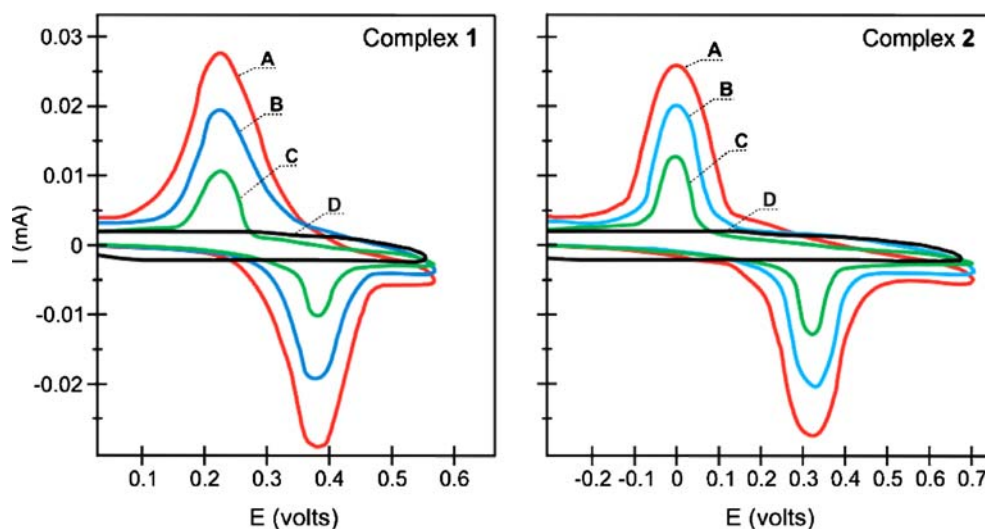
Table 2 Electrochemical data of the copper compounds

Compound	E_{pc} (mV) versus NHE	E_{pa} (mV) versus NHE	$E_{1/2}$ (mV)[a]
Complex **1**	224	382	303
Complex **2**	−20	322	151
Cu(NO$_3$)$_2$	222	362	292

NHE normal hydrogen electrode
[a]$E_{1/2} = (E_{pa} + E_{pc})/2$

effectively catalyze O$_2^{\bullet-}$ dismutation, with the formation of H$_2$O$_2$, according to Eqs. 1 and 2.
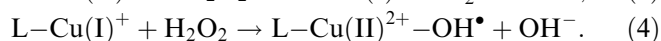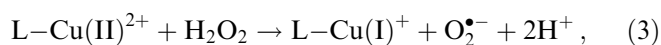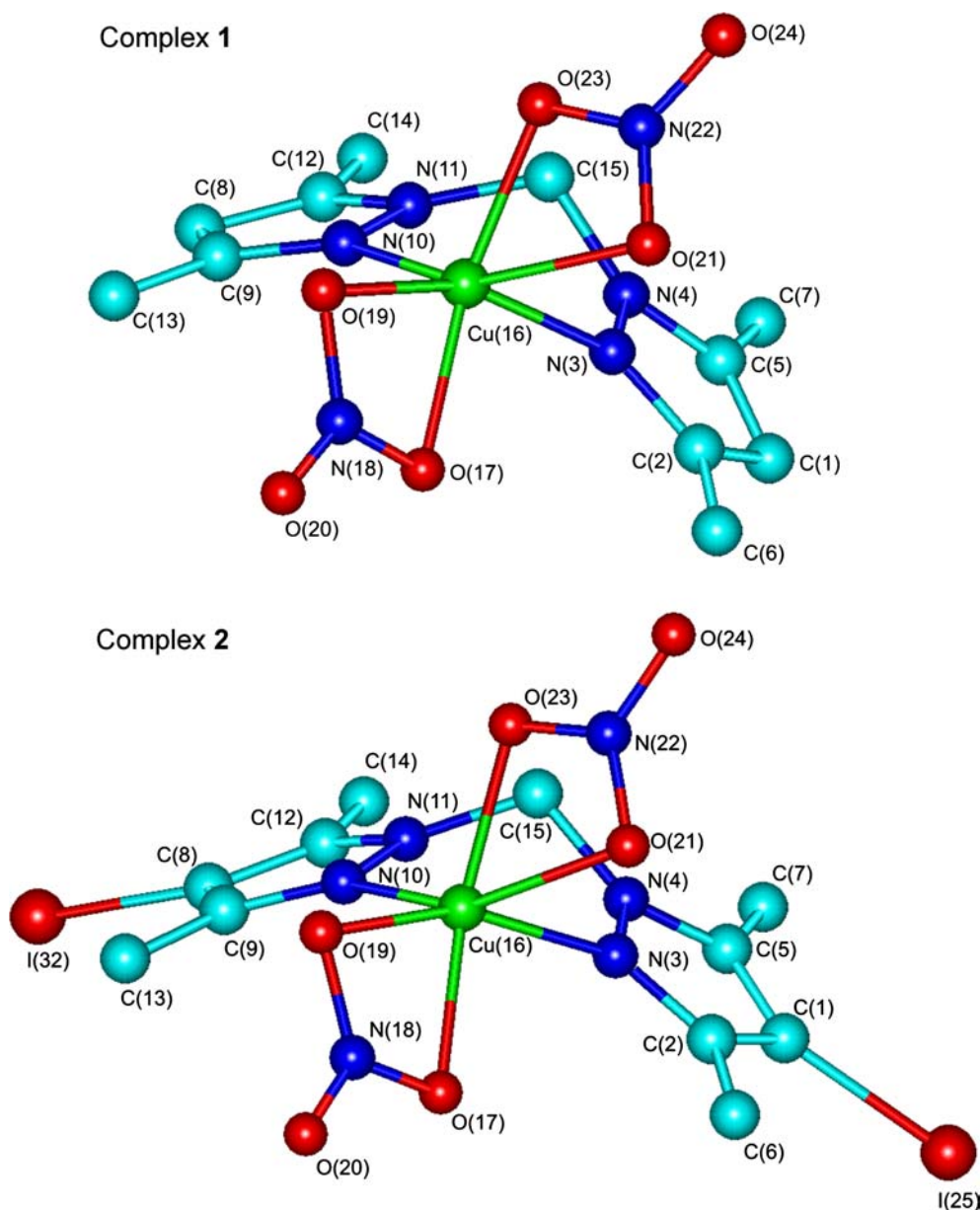
Peroxidase-like activity

The ability of Cu(II) complexes to catalyze decomposition of H$_2$O$_2$ has been extensively investigated owing to implications for many biological processes and their high reactivity in comparison with other transition metal complexes [50–53]. Cu,Zn-SOD is able to act as a non-specific peroxidase, and it is assumed that OH$^\bullet$ generation may occur during the reactions of H$_2$O$_2$ with Cu,Zn-SOD and small SOD mimetics [53, 54]. It has been documented that the catalytic activity of Cu(II) in the luminescence reaction of luminol and H$_2$O$_2$ increased when Cu(II) interacted with bovine albumin [55] or microspheres [56]. Here we investigated the peroxidase-like activity of the Cu(II) compounds, as determined by monitoring luminescence emission in H$_2$O$_2$/luminol and H$_2$O$_2$/L-012 systems.

In the absence of Cu(II) compounds, addition of H$_2$O$_2$ to luminol (data not shown) or L-012 (Fig. 5c) resulted in a very weak luminescence signal, which was similar to or slightly above the signal measured with luminol or L-012 alone (Fig. 5c, inset). In contrast, addition of either Cu(II) compound to the H$_2$O$_2$/luminol system resulted in a concentration-dependent

luminescence signal, with complex **1** being the more potent and complex **2** being similar to Cu(NO$_3$)$_2$ (Fig. 5a). Similarly, addition of the Cu(II) compounds to the H$_2$O$_2$/L-012 system also caused a concentration-dependent luminescence signal, with potencies of complex **1** > complex **2** ≈ Cu(NO$_3$)$_2$ (Fig. 5b, c). As shown in Fig. 5c, the luminescence signal induced by complex **1** reached maximal values at approximately 15 min and remained at this plateau without change in intensity for more than 8 h. The signal induced by complex **1** at concentrations of 1.5–6 μM was approximately 20–25 times greater than that induced by Cu(NO$_3$)$_2$ or complex **2**, demonstrating that the complex of L$_1$ and Cu(II) can strongly catalyze a peroxidase-like reaction. Additionally, these results suggest that H$_2$O$_2$ did not cause decomposition of the complex to release copper ions, since complex **1** catalyzed a much greater response than Cu(NO$_3$)$_2$ alone. This conclusion is further supported by experiments suggesting in situ complex formation in reactions containing L$_1$ and Cu(NO$_3$)$_2$. As shown in Fig. 6, the luminescence signal generated by the reaction of Cu(NO$_3$)$_2$ with H$_2$O$_2$ was increased by the addition of increasing concentrations of L$_1$, indicating that complex **1** may form in situ. It should be noted that the luminescence signal was not enhanced by similar concentrations of L$_1$ in the absence of Cu(NO$_3$)$_2$ (data not shown).

Consistent with previous reports that SOD can catalyze the formation of "free" and/or metal-bound OH$^\bullet$ [55, 57], SOD exhibited peroxidase-like activity in the H$_2$O$_2$/L-012 assay, resulting in L-012 oxidation (Fig. 5c). However, a longer lag time was necessary for initiation of maximal peroxidase-like activity by SOD in comparison with the Cu(II) compounds. These data can be interpreted in terms of the reduction of the pyrazole-bound Cu(II) to Cu(I) by H$_2$O$_2$, followed by a Fenton-type reaction of Cu(I) with additional H$_2$O$_2$, as has been proposed for other copper complexes [52] and Cu,Zn-SOD [57, 58]:

Fig. 3 Molecular modeling of Cu(II) complexes. Molecular representations of complexes **1** and **2** determined by ab initio geometry optimizations. Atoms are labeled, and hydrogen atoms are omitted for clarity

$$L-Cu(II)^{2+} + H_2O_2 \rightarrow L-Cu(I)^+ + O_2^{\bullet-} + 2H^+, \quad (3)$$

$$L-Cu(I)^+ + H_2O_2 \rightarrow L-Cu(II)^{2+}-OH^{\bullet} + OH^-. \quad (4)$$

Interestingly, addition of SOD to reactions of H_2O_2/L-012/complex **1** and H_2O_2/L-012/$Cu(NO_3)_2$ resulted in opposite effects, inhibition versus activation, respectively (Fig. 5c). Although the additional effects of SOD were relatively small, the results suggest the possibility that $O_2^{\bullet-}$ may have different effects on these two systems. It is also possible that $O_2^{\bullet-}$ formed from the decomposition of H_2O_2 by complex **1** (Eq. 3) attacks the L-012 probe or generates pyrazole-bonded univalent copper (Eq. 1), which can be used in the reaction in Eq. (4). As previously reported, $O_2^{\bullet-}$ also causes L-012-dependent luminescence [59], and the relatively higher SOD-like activity

of complex **1** may result in a more efficient scavenging of any $O_2^{\bullet-}$ generated in the system.

Effect on peroxynitrite decomposition

Peroxynitrite, a biologically relevant oxidizing and nitrating species, is produced by the nearly diffusion limited reaction between nitric oxide (NO) and $O_2^{\bullet-}$ [60]. The rate of decomposition of peroxynitrite in strongly basic solutions is enhanced by addition of Cu(II) ions [61, 62]. On the other hand, bidentate and polydentate Cu(II) ligands (glycine, 2,2′-bipyridyl, EDTA) all inhibited the catalytic action of free Cu(II) ions [61, 63]. Here we evaluated whether peroxynitrite decomposition

Table 3 Selected bond distances, bond orders, and angles for complex **1** determined by ab initio 3-21G geometry optimizations

Bond	Length (Å)	Bond order	Bond	Length (Å)	Bond order
Cu(16)–O(17)	2.025	0.267	N(3)–N(4)	1.390	0.855
Cu(16)–O(19)	2.084	0.254	C(2)–N(3)	1.316	1.280
Cu(16)–O(21)	2.465	0.113	C(1)–C(2)	1.412	1.035
Cu(16)–O(23)	1.970	0.328	C(1)–C(5)	1.369	1.315
Cu(16)–N(3)	2.028	0.305	C(5)–N(4)	1.349	1.264
Cu(16)–N(10)	2.107	0.339	N(4)–C(15)	1.451	0.786

Bond	Angle (°)	Bond	Angle (°)
N(3)–Cu(16)–N(10)	91.327	N(10)–Cu(16)–O(17)	108.575
N(3)–Cu(16)–O(17)	92.296	N(10)–Cu(16)–O(19)	100.474
N(3)–Cu(16)–O(19)	157.294	N(10)–Cu(16)–O(21)	155.297
N(3)–Cu(16)–O(21)	83.622	N(10)–Cu(16)–O(23)	96.510
N(3)–Cu(16)–O(23)	94.609	N(4)–C(15)–N(11)	111.593
O(17)–Cu(16)–O(19)	65.631	O(17)–Cu(16)–O(21)	95.809
O(17)–Cu(16)–O(23)	153.802	O(19)–Cu(16)–O(21)	92.997
O(19)–Cu(16)–O(23)	103.144	O(21)–Cu(16)–O(23)	60.029
O(21)–N(22)–O(23)	116.387	O(17)–N(18)–O(19)	113.184

Table 4 Selected bond distances, bond orders, and angles for complex **2** determined by ab initio 3-21G geometry optimizations

Bond	Length (Å)	Bond order	Bond	Length (Å)	Bond order
Cu(16)–O(17)	1.930	0.271	N(3)–N(4)	1.459	0.872
Cu(16)–O(19)	1.947	0.255	C(2)–N(3)	1.375	1.294
Cu(16)–O(21)	2.068	0.117	C(1)–C(2)	1.422	1.069
Cu(16)–O(23)	1.949	0.327	C(1)–C(5)	1.377	1.161
Cu(16)–N(3)	1.979	0.301	C(5)–N(4)	1.405	1.246
Cu(16)–N(10)	2.077	0.328	N(4)–C(15)	1.481	0.783
C(1)–I(25)	1.949	1.225	C(8)–I(32)	1.949	1.240

Bond	Angle (°)	Bond	Angle (°)
N(3)–Cu(16)–N(10)	91.483	N(10)–Cu(16)–O(17)	107.396
N(3)–Cu(16)–O(17)	94.228	N(10)–Cu(16)–O(19)	99.531
N(3)–Cu(16)–O(19)	106.518	N(10)–Cu(16)–O(21)	148.861
N(3)–Cu(16)–O(21)	93.885	N(10)–Cu(16)–O(23)	85.487
N(3)–Cu(16)–O(23)	97.459	N(4)–C(15)–N(11)	109.503
O(17)–Cu(16)–O(19)	67.213	O(17)–Cu(16)–O(21)	102.761
O(17)–Cu(16)–O(23)	162.381	O(19)–Cu(16)–O(21)	84.985
O(19)–Cu(16)–O(23)	99.376	O(21)–Cu(16)–O(23)	63.410
O(21)–N(22)–O(23)	63.410	O(17)–N(18)–O(19)	112.026

Table 5 Energies of boundary orbitals and heats of formation of the Cu(II) complexes

Compound	E_{HOMO} (eV)	E_{LUMO} (eV)	Heat of formation (kcal mol^{-1})	
			Monodentate NO_3^-	Bidentate NO_3^-
Complex **1**	−10.045	−0.0250	−57.91	−101.09
Complex **2**	−9.357	−0.0146	7.97	−38.82

was catalyzed by the Cu(II) compounds under investigation.

Peroxynitrite decay rates were measured as a function of initial peroxynitrite concentration at fixed concentrations of Cu(II) compounds (3.0 μM) in solution at pH 10.9. The primary mechanism of peroxynitrite decomposition by Cu(II) compounds under these conditions is Cu(II)-induced homolysis of the O–O bond in peroxynitrous acid, yielding the radical intermediate and strong oxidizing species, Cu(III) [61, 63]. Initial velocity data, when corrected for background decay, were found to fit Michaelis–Menten kinetics, and the

Table 6 Effect of Cu(II) compounds on $O_2^{\bullet-}$ and urate production

Compound	Xanthine/xanthine oxidase system		Phenazine methosulfate/NADH system		Electrochemical production of $O_2^{\bullet-}$
	Nitro blue tetrazolium reduction IC_{50} (μM)	Urate production IC_{50} (μM)	IC_{50} (μM)	k_{cat} (M^{-1} s^{-1})	IC_{50} (μM)
Complex **1**	0.79	0.64	0.45	6.6×10^6	1.35
Complex **2**	2.14	1.38	0.79	3.8×10^6	1.93
Cu(NO₃)₂	2.33	2.7	1.1	2.7×10^6	2.35
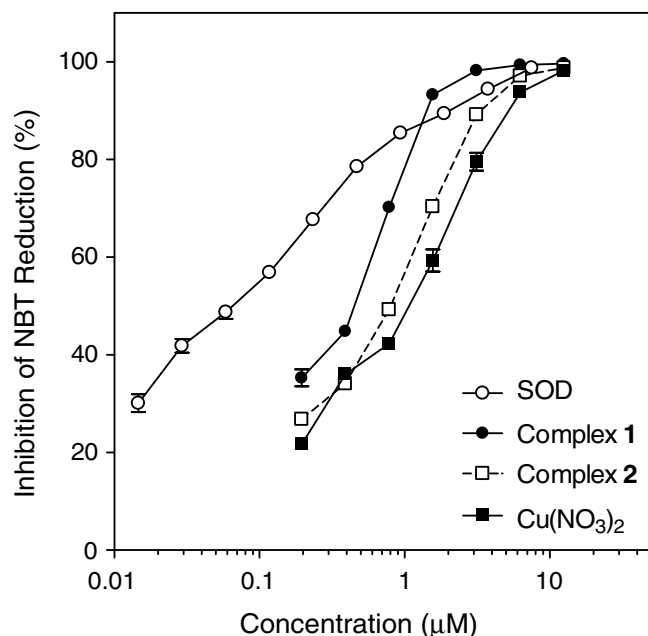
Fig. 4 Analysis of superoxide dismutase (*SOD*) like activity of Cu(II) complexes in a nonenzymatic $O_2^{\bullet-}$-generating system. The indicated concentrations of complex **1** (*filled circles*), complex **2** (*filled squares*), Cu(NO₃)₂ (*open squares*), and SOD (*open circles*) were added to the phenazine methosulfate/NADH system, and nitro blue tetrazolium reduction was determined, as described. The data are expressed as means $\pm$ the standard deviation (*SD*); $N = 3$. A representative experiment from three independent experiments is shown

"dissociation" constant of the catalyst/substrate complex (K_m) and the limiting turnover rate of the complex ($k_2 = V_{max}$/catalyst) were obtained from Lineweaver–Burk plots (Table 7). These values, along with the calculated bimolecular catalytic rate constant (i.e., $k_{cat} = k_2/K_m$), indicated complex **1** was much more efficient than either complex **2** or Cu(NO₃)₂ in degrading peroxynitrite, with k_{cat} values of 6.4, 1.9, and 3.0×10^5 M^{-1} s^{-1}, respectively.

The oxidation of fluorogenic probes (dichlorodihydrofluorescein and DHR 123) by peroxynitrite occurs via free-radical intermediates formed during peroxynitrite decomposition [64, 65]. As shown in Fig. 7, the rate of DHR 123 oxidation was enhanced by the Cu(II) compounds in the order complex **1** > > complex **2** > Cu(NO₃)₂, suggesting $NO_2^{\bullet}$ formed during peroxynitrite decomposition by pyrazole–Cu(II) complexes was responsible for the enhanced rhodamine formation. Indeed, the participation of $NO_2^{\bullet}$ in DHR 123 oxidation has been shown [65]. The regeneration of Cu(II) from Cu(III) in the pyrazole complex could also result in the oxidation of DHR to rhodamine.

The ability of transition-metal-containing complexes to protect biological systems against peroxynitrite-mediated injury depends primarily on (1) rate constants for reaction of complexes with peroxynitrite, (2) rate constants for complex recycling, and (3) how well the complexes quench the resulting reactive intermediates [66]. In the present study, we show k_{cat} values for peroxynitrite decomposition by complexes **1** and **2** were on the same order of magnitude as reported for Fe^{3+} porphyrins [66]. However, with K_m values in the millimolar range, it is possible that these Cu(II) complexes would not be effective against peroxynitrite-mediated injury in biological systems, where peroxynitrite concentrations are estimated in the micromolar range [67].

Effect on ROS produced by phagocytes in whole blood (ex vivo)

Exogenous SOD is effective only in removing $O_2^{\bullet-}$ present in extracellular compartments because it is a large, polar compound that does not readily cross cell membranes [68]. Thus, low molecular weight copper complexes, which can cross cell membranes and reach intracellular sites of $O_2^{\bullet-}$ generation while retaining SOD-like activity, have been suggested to be more desirable drug candidates [69]. To evaluate SOD-like activity of the Cu(II) complexes on $O_2^{\bullet-}$ produced by phagocytes and the ability of the complexes to penetrate cells and reach intracellular $O_2^{\bullet-}$-generating sites, we performed assays using diluted human whole blood (ex vivo system). In this system, ROS were primarily generated by neutrophils [70]. Addition of the Cu(II) compounds resulted in a concentration-dependent inhibition of spontaneous (nonstimulated blood cells) and PMA-induced chemiluminescence, indicating these complexes were effective ROS scavengers in this ex vivo system (Fig. 8a, b). Complex **1** was the most active compound and inhibited ROS generation at nanomolar concentrations. In these systems, $O_2^{\bullet-}$ was generated extracellularly, as SOD (1 U ml⁻¹) also completely inhibited the
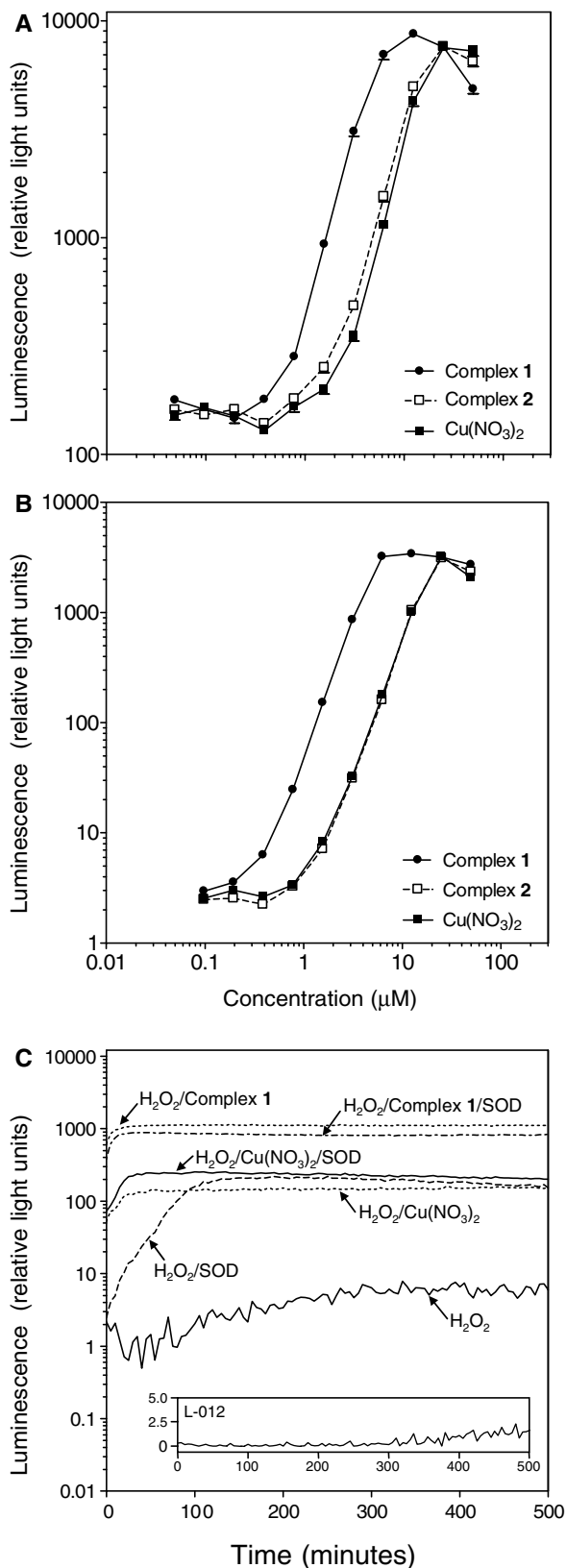
A

B

C

Fig. 5 Analysis of peroxidase-like activity of Cu(II) complexes. The indicated concentrations of complex **1** (*circles*), complex **2** (*filled squares*), and Cu(NO$_3$)$_2$ (*open squares*) were added to assay mixtures consisting of 250 μM H$_2$O$_2$/25 μM luminol (**a**) or 250 μM H$_2$O$_2$/100 μM 8-amino-5-chloro-7-phenylpyridol[3,4-*d*]pyridazine-1,4(2*H*,3*H*)-dione (*L-012*) (**b**) and luminescence was measured, as described. The data are presented as integrated luminescence (over the first 30 min) versus test compound concentration. **c** The kinetics of peroxidase-like responses was monitored over the indicated time period in H$_2$O$_2$/L-012 reactions containing 6.25 μM complex **1** or Cu(NO$_3$)$_2$ with or without 100 U ml^{-1} SOD, as indicated. Samples of 250 μM H$_2$O$_2$ alone with or without 100 U ml^{-1} SOD are included for comparison (indicated as *H$_2$O$_2$* and *H$_2$O$_2$/SOD*). The *inset* shows background signal due to L-012 alone. The data are expressed as means ± SD; *N* = 3. In **a–c**, a representative experiment from three independent experiments is shown
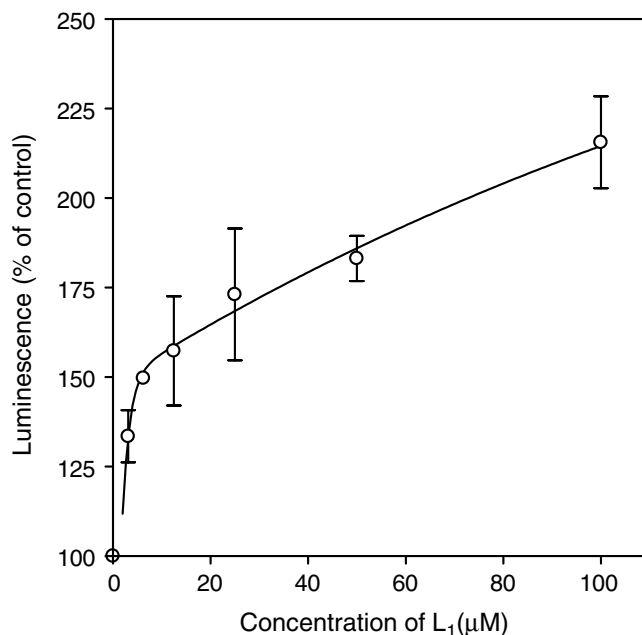
Fig. 6 In situ formation of complex **1**. The indicated concentrations of L$_1$ were added to reaction mixtures containing 1 μM Cu(NO$_3$)$_2$ and 250 μM H$_2$O$_2$/100 μM L-012, and luminescence was measured. The data are expressed as means ± SD; *N* = 3. A representative experiment from three independent experiments is shown

Table 7 Catalytic rate constants for peroxynitrite decomposition by Cu(II) compounds

Compound	K_m (mM)	k_2 (s^{-1})	k_{cat} (M^{-1} s^{-1})
Complex 1	15.9	1.0×10^4	6.4×10^5
Complex 2	1.1	2.0×10^2	1.9×10^5
Cu(NO$_3$)$_2$	2.3	7.0×10^2	3.0×10^5

chemiluminescence response. In contrast, zymosan-stimulated chemiluminescence was inhibited to approximately 50% at same concentration of SOD (data not shown), suggesting O$_2^{\bullet-}$ was also being generated inside these cells [71]. Indeed, it was reported previously that neutrophils generate both extracellular and intracellular
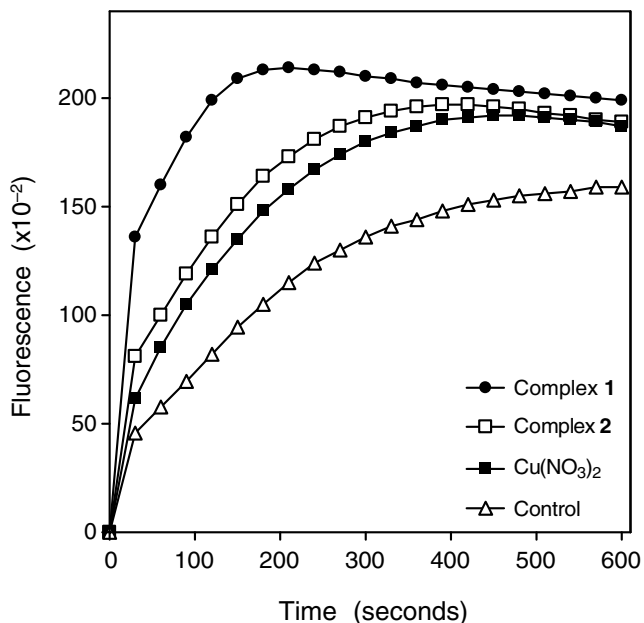
Fig. 7 Analysis of peroxynitrite decomposition by Cu(II) complexes. Peroxynitrite (80 μM) was added to reactions containing 15 μM dihydrorhodamine (*DHR*) 123 and complex **1** (*circles*), complex **2** (*filled squares*), or Cu(NO$_3$)$_2$ (*open squares*) (1.5 μM each) at 25 °C, and fluorescence ($\lambda_{ex}=485$ nm, $\lambda_{em}=538$ nm) was measured immediately. Control reactions contained only peroxynitrite and DHR (*triangles*). A representative experiment from three independent experiments is shown

Qualifications of an SOD mimic

To act as a qualified SOD mimic (in vitro), a compound needs to have the following properties [74]: (1) the
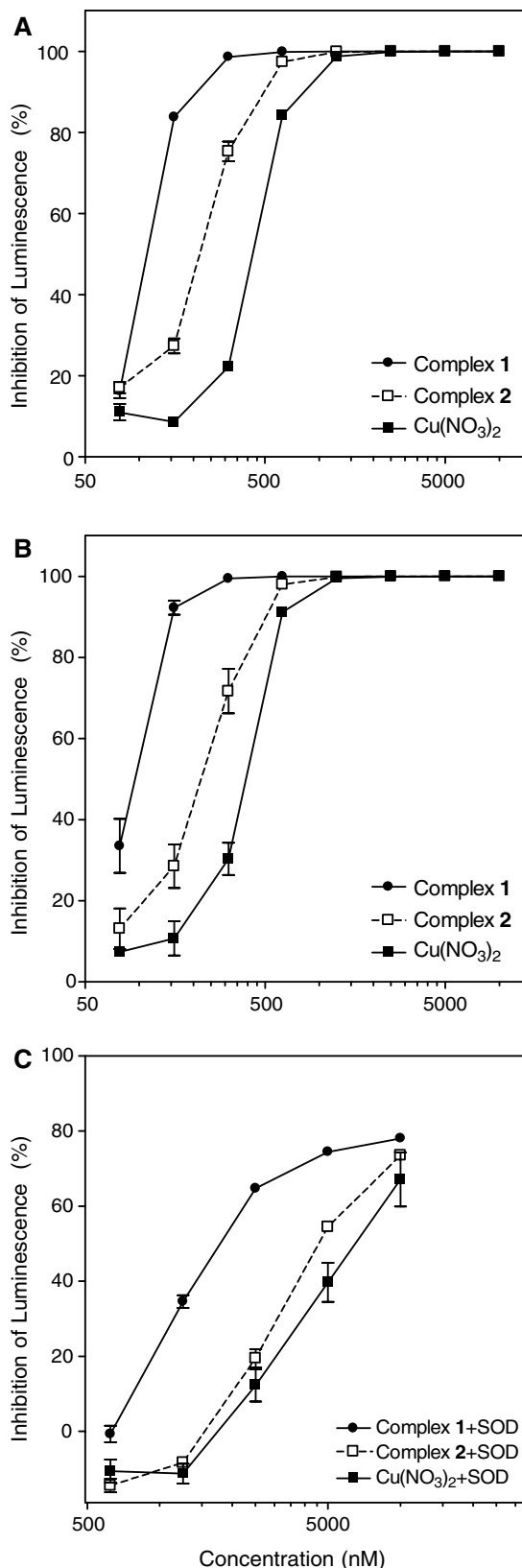

ROS during phagocytosis of zymosan particles and that only extracellular O$_2^{\bullet-}$ is removed by SOD [71, 72]. Thus, comparison of chemiluminescence responses in the presence and absence of SOD provides an accurate measurement of intracellular O$_2^{\bullet-}$ production [71, 73]. Using this approach, we evaluated intracellular SOD-like activity of the Cu(II) compounds. Diluted human blood was incubated with opsonized zymosan for 15 min, and L-012-dependent chemiluminescence was measured in the presence of SOD (1 U ml^{-1}) and the indicated concentrations of Cu(II) compounds (Fig. 8c). As shown in Fig. 8c, complex **1** was also an active intracellular O$_2^{\bullet-}$ scavenger. On the basis of these results, complex **1** can be considered as a promising protective agent against ROS generated by phagocytic granulocytes.

Fig. 8 Evaluation of SOD-like activity of Cu(II) complexes on neutrophil-derived reactive oxygen species. Effects of the indicated concentrations of complex **1** (*circles*), complex **2** (*filled squares*), and Cu(NO$_3$)$_2$ (*open squares*) on spontaneous (**a**), phorbol-12-myristate-13-acetate (200 nM) (**b**), and opsonized zymosan (100 μg ml^{-1}) (**c**) induced L-012 chemiluminescence in diluted human blood (1:1,000 in Hanks's balanced-salt solution) were determined, as described. In **c**, 1 U ml^{-1} SOD was included to eliminate any extracellular O$_2^{\bullet-}$. The data are expressed as means ± SD; $N=3$. In **a**–**c**, a representative experiment from three independent experiments is shown

512

Table 8 Effect of pyrazole ligands and their Cu(II) complexes on cell viability

Concentration (μM)	L_1	L_2	Complex 1	Complex 2
0.625	97.7 ± 12.0	102.0 ± 4.1	98.0 ± 2.6	99.6 ± 4.2
1.25	93.5 ± 9.7	99.1 ± 3.4	99.4 ± 0.7	98.9 ± 1.0
2.5	97.2 ± 5.2	101.0 ± 1.0	97.7 ± 0.9	96.3 ± 0.5
5	95.2 ± 7.1	98.2 ± 2.3	96.9 ± 1.0	96.3 ± 2.6
10	95.9 ± 1.4	94.3 ± 2.9	94.5 ± 0.5	95.9 ± 0.9
20	92.4 ± 7.1	94.8 ± 1.0	93.2 ± 1.4	93.1 ± 0.7
40	94.9 ± 3.4	93.7 ± 2.5	91.1 ± 1.6	90.4 ± 3.5

Results are expressed as the percentage of cell viability measured in untreated, control cells and are presented as means $\pm$ the standard deviation; $N = 3$. A representative experiment from three independent experiments is shown

compound should have a relatively long metabolic half-life for it to carry out its SOD-like activity, (2) it should be able to penetrate into the cells to reach the target region, and (3) it should not be toxic at the concentrations needed for SOD-like activity. The data presented here demonstrate that the Cu(II) compounds meet qualifications 1 and 2. For instance, significant differences between the UV–vis spectra of the ligands and $Cu(NO_3)_2$ versus the Cu(II) complexes suggest the stability of the complexes under experimental conditions is rather high. In cell-based assay systems, the Cu(II) complexes exhibited much higher SOD-like activity when compared with $Cu(NO_3)_2$, again indicating the complexes retain their structural integrity in a biologically relevant environment. We also demonstrated that Cu(II) complexes **1** and **2** can penetrate human neutrophils and scavenge intracellular ROS. To address requirement 3, we performed a cell viability/proliferation test in J774.A1 macrophages treated with Cu(II) complexes. Proliferation and viability of J774.A1 cells were not affected by treatment of the cells with L_1 and L_2 or their Cu(II) complexes over a wide concentration range (0.625–40 μM) (no significant differences from the control were observed, $P > 0.05$) (Table 8).

Conclusion

We reported the preparation of two new Cu(II) pyrazolylalkane complexes: bis(3,5-dimethyl-1-pyrazolyl)methanedinitratocopper(II) (complex **1**) and bis(4-iodo-3,5-dimethyl-1-pyrazolyl)methanedinitratocopper(II) (complex **2**). The starting compound bis(3,5-dimethyl-1-pyrazolyl)methane (L_1) was synthesized using a novel procedure involving dibromomethane double alkylation by 3,5-dimethylpyrazole in a superbasic medium. Characterization of the synthesized Cu(II) complexes demonstrated a 1:1 stoichiometry, with bidentate coordination modes of organic ligand and nitrate ions. Additionally, an octahedral geometry was established for the central copper ion.

The complexes were characterized using spectroscopic and electrochemical methods in solution and in the solid state. Cyclic voltammetric data showed both complexes can be oxidized by $O_2^{\bullet-}$ scavengers. Complex **1** was the most stable and effective SOD-like compound, with activity similar to that previously reported for other SOD-like Cu(II) complexes. In addition, Cu(II) complexes **1** and **2** can penetrate human neutrophils and decompose intracellular ROS without causing detectable cytotoxic effects. Thus, these complexes represent useful models for investigating SOD function.

References

1. Quinn MT, Gauss KA (2004) J Leukocyte Biol 76:760–781
2. Fang FC (2004) Nat Rev Microbiol 2:820–832
3. Serhan CN, Savill J (2005) Nat Immunol 6:1191–1197
4. McCord JM, Edeas MA (2005) Biomed Pharmacother 59:139–142
5. Fridovich I (1998) J Exp Biol 201:1203–1209
6. Matés JM, Pérez-Gómez C, De Castro IN (1999) Clin Biochem 32:595–603
7. Pong K (2003) Expert Opin Biol Ther 3:127–139
8. Tabbi G, Driessen WL, Reedijk J, Bonomo RP, Veldman N, Spek AL (1997) Inorg Chem 36:1168–1175
9. Tian Y, Fang Y, Sun C, Shen W, Luo Q, Shen M (1993) Biochem Biophys Res Commun 191:646–653
10. Trofimenko S (1993) Chem Rev 93:943–980
11. Mukherjee R (2000) Coord Chem Rev 203:151–218
12. Ballesteros P, Claramunt RM, Lopez MC, Elguero J, Gomezalarcon G (1988) Chem Pharm Bull (Tokyo) 36:2036–2041
13. Supuran CT, Claramunt RM, Lavandera JL, Elguero J (1996) Biol Pharm Bull 19:1417–1422
14. Broomhead JA, Camm G, Sterns M, Webster L (1998) Inorg Chim Acta 271:151–159
15. Pettinari C, Pettinari R (2005) Coord Chem Rev 249:525–543
16. Hammes BS, Carrano CJ (2000) Chem Commun 17:1635–1636
17. Beck A, Weibert B, Burzlaff N (2001) Eur J Inorg Chem 2:521–527
18. Higgs TC, Carrano CJ (1997) Inorg Chem 36:291–297
19. Higgs TC, Carrano CJ (1997) Inorg Chem 36:298–306
20. Higgs TC, Ji D, Czernuscewicz RS, Carrano CJ (1998) Inorg Chim Acta 273:14–23
21. Reedijk J, Verbiest J (1979) Transition Met Chem 4:239–243
22. Mesubi MA, Anumba FO (1985) Transition Met Chem 10:5–8
23. Potapov AS, Khlebnikov AI (2003) Izv Vuzov Ser Khim Khim Tekhnol 7:66–71
24. Patel RN, Singh N, Shukla KK, Gundla VL, Chauhan UK (2005) J Inorg Biochem 99:651–663
25. Hypercube (2002) HyperChem computational chemistry: molecular visualization and simulation, release 7 for Windows. Hypercube, Edmonton
26. Huguet AI, Manez S, Alcaraz MJ (1990) Z Naturforsch 45:19–24
27. Bielski BHJ, Richter HW (1977) J Am Chem Soc 99:3019–3023
28. Durot S, Policar C, Cisnetti F, Lambert F, Renault JP, Pelosi G, Blain G, Korri-Youssoufi H, Mahy JP (2005) Eur J Inorg Chem 17:3513–3523

29. Bindoli A, Valente M, Cavallini L (1985) Pharmacol Res Commun 17:831–839
30. Korotkova EI, Karbainov YA, Avramchik OA (2003) Anal Bioanal Chem 375:465–468
31. Imada I, Sato EF, Miyamoto M, Ichimori Y, Minamiyama Y, Konaka R, Inoue M (1999) Anal Biochem 271:53–58
32. Yamazaki K, Fukuda K, Matsukawa M, Hara F, Matsushita T, Yamamoto N, Yoshida K, Munakata H, Hamanishi C (2003) Arthritis Rheum 48:3151–3158
33. Bohle DS, Glassbrenner PA, Hansert B (1996) Methods Enzymol 269:302–311
34. Glebska J, Koppenol WH (2003) Free Radic Biol Med 35:676–682
35. Crouch SP, Kozlowski R, Slater KJ, Fletcher J (1993) J Immunol Methods 160:81–88
36. Julia S, Sala P, Delmazo J, Sancho M, Ochoa C, Elguero J, Fayet JP, Vertut MC (1982) J Heterocycl Chem 19:1141–1145
37. Claramunt RM, Hernandez H, Elguero J, Julia S (1983) Bull Soc Chim Fr 1–2:5–10
38. Tretyakov EV, Vasilevsky SF (1995) Mendeleev Commun 6:233–234
39. Nakamoto K (1986) Infrared spectra of inorganic and coordination compounds. Wiley, New York
40. Lever ABP (1984) Inorganic electronic spectra. Elsevier, Amsterdam
41. Zhang L-Z, Ma SL, Shen A-Y, Fu M, Zhang L-J, Liu X (2003) Pol J Chem 77:837–844
42. Li D, Li S, Yang D, Yu J, Huang J, Li Y, Tang W (2003) Inorg Chem 42:6071–6080
43. Bertini I, Gatteschi D, Scozzafava A (1979) Coord Chem Rev 29:67–84
44. Schuitema AM, Engelen M, Koval IA, Gorter S, Driessen WL, Reedijk J (2001) Inorg Chim Acta 324:57–64
45. Jitsukawa K, Harata M, Arii H, Sakurai H, Masuda H (2001) Inorg Chim Acta 324:108–116
46. Filimonov VD, Karbainov YA, Korotkova EI, Bashkatova NV, Volovodenko AV (2002) Izv Vuzov Ser Khim Khim Tekhnol 3:75–79
47. Thomas CE, Ohlweiler DF, Carr AA, Nieduzak TR, Hay DA, Adams G, Vaz R, Bernotas RC (1996) J Biol Chem 271:3097–3104
48. Policar C, Durot S, Lambert F, Cesario M, Ramiandrasoa F, Morgenstern-Badarau I (2001) Eur J Inorg Chem 7:1807–1818
49. Weser U, Schubotz LM (1981) J Mol Catal 13:249–261
50. Korytowski W, Sarna T (1990) J Biol Chem 265:12410–12416
51. Jezowska-Bojczuk M, Lesniak W, Bal W, Kozlowski H, Gatner K, Jezierski A, Sobczak J, Mangani S, Meyer-Klaucke W (2001) Chem Res Toxicol 14:1353–1362
52. Salem IA, El-Sheikh MY, Younes AAA, Zaki AB (2000) Int J Chem Kinet 32:667–675
53. Ueda J, Takai M, Shimazu Y, Ozawa T (1998) Arch Biochem Biophys 357:231–239
54. Yim MB, Chock PB, Stadtman ER (1990) Proc Natl Acad Sci USA 87:5006–5010
55. Li ZP, Fan SS, Zhang LN, Wang FC (2004) Anal Sci 20:1327–1331
56. Tsukagoshi K, Sumiyama M, Nakajima R, Nakayama M, Maeda M (1998) Anal Sci 14:409–412
57. Hodgson EK, Fridovich I (1975) Biochemistry 14:5294–5299
58. Kladna A, boul-Enein HY, Kruk I (2003) Free Radic Biol Med 34:1544–1554
59. Sohn HY, Gloe T, Keller M, Schoenafinger K, Pohl U (1999) J Vasc Res 36:456–464
60. Beckman JS, Koppenol WH (1996) Am J Physiol Cell Physiol 271:C1424–C1437
61. Hughes MN, Nicklin HG, Sackrule WA (1971) J Am Chem Soc 3722–3725
62. AlAjlouni AM, Gould ES (1997) Inorg Chem 36:362–365
63. Babich OA, Gould ES (2002) Res Chem Intermed 28:79–85
64. Jourd'heuil D, Jourd'heuil FL, Kutchukian PS, Musah RA, Wink DA, Grisham MB (2001) J Biol Chem 276:28799–28805
65. Wrona M, Patel K, Wardman P (2005) Free Radic Biol Med 38:262–270
66. Crow JP (1999) Arch Biochem Biophys 371:41–52
67. Carreras MC, Pargament GA, Catz SD, Poderoso JJ, Boveris A (1994) FEBS Lett 341:65–68
68. Fattman CL, Schaefer LM, Oury TD (2003) Free Radic Biol Med 35:236–256
69. Wada K, Fujibayashi Y, Yokoyama A (1994) Arch Biochem Biophys 310:1–5
70. Lojek A, Kubala L, Cizova H, Ciz M (2002) Luminescence 17:1–4
71. Granfeldt D, Dahlgren C (2001) Inflammation 25:165–169
72. Bassoe CF, Li NY, Ragheb K, Lawler G, Sturgis J, Robinson JP (2003) Cytometry 51B:21–29
73. Riber U, Lind P (1999) Vet Immunol Immunopathol 67:259–270
74. Czapski G, Goldstein S (1990) Adv Exp Med Biol 264:45–50